REPORT DOCUMENTATION PAGE

Form Approved
OMB No. 0704-01-0188

1. REPORT DATE *(DD-MM-YYYY)*	2. REPORT TYPE	3. DATES COVERED *(From - To)*
01-08-2006	REPRINT	

4. TITLE AND SUBTITLE
Electron-Ion Beam Coupling Through Collective Interactions

5a. CONTRACT NUMBER

5b. GRANT NUMBER

5c. PROGRAM ELEMENT NUMBER
62601F

6. AUTHORS
Adrian Wheelock
David L. Cooke
Nikolaos A. Gatsonis*

5d. PROJECT NUMBER
1010

5e. TASK NUMBER
RS

5f. WORK UNIT NUMBER
A1

7. PERFORMING ORGANIZATION NAME(S) AND ADDRESS(ES)
Air Force Research Laboratory /VSBXT
29 Randolph Road
Hanscom AFB, MA 01731-3010

8. PERFORMING ORGANIZATION REPORT NUMBER
AFRL-VS-HA-TR-2006-1068

9. SPONSORING/MONITORING AGENCY NAME(S) AND ADDRESS(ES)

10. SPONSOR/MONITOR'S ACRONYM(S)
AFRL/VSBXR

11. SPONSOR/MONITOR'S REPORT NUMBER(S)

12. DISTRIBUTION/AVAILABILITY STATEMENT
Approved for public release; distribution unlimited.

13. SUPPLEMENTARY NOTES
Presented at 42nd AIAA Joint Propulsion Conference, Sacramento, CA, 12 July 2006. Also available as AIAA-06-5024. *Worcester Polytechnic Institute, Worcester, MA 01609

14. ABSTRACT

Neutralization of ion beams in electric propulsion applications is a well-known phenomenon. The physics behind the robust matching of both ion and electron currents and densities are not. With electric propulsion devices moving into micro and macro regimes with colloids, FEEPs, and thruster arrays, thruster-neutralization interactions are under increasing scrutiny. It is shown that Coulomb collisions, which can act to match velocities through strong ion-electron collisions between particles with low relative velocities, are far too slow to explain the phenomenon. Further examination of the strong beam-plasma, or Buneman, instability yields a candidate for the neutralization mechanism. Differences in simulations from analytic theory are discussed. .

15. SUBJECT TERMS
Electric propulsion
Coulomb collisions
Neutralization of ion beams

16. SECURITY CLASSIFICATION OF:			17. LIMITATION OF ABSTRACT	18. NUMBER OF PAGES	19a. NAME OF RESPONSIBLE PERSON
a. REPORT	b. ABSTRACT	c. THIS PAGE			David L. Cooke
UNCL	UNCL	UNCL	UNL		19B. TELEPHONE NUMBER *(Include area code)*

ELECTRON-ION BEAM COUPLING THROUGH COLLECTIVE INTERACTIONS

Adrian Wheelock* and David L. Cooke†
Air Force Research Laboratory, Space Vehicles Directorate, Hanscom AFB, MA 01731

Nikolaos A. Gatsonis‡
Mechanical Engineering Department, Worcester Polytechnic Institute, Worcester, MA 01609

Neutralization of ion beams in electric propulsion applications is a well-known phenomenon. The physics behind the robust matching of both ion and electron currents and densities are not. With electric propulsion devices moving into micro and macro regimes with colloids, FEEPs, and thruster arrays, thruster-neutralizer interactions are under increasing scrutiny. It is shown that Coulomb collisions, which can act to match velocities through strong ion-electron collisions between particles with low relative velocities, are far too slow to explain the phenomenon. Further examination of the strong beam-plasma, or Buneman, instability yields a candidate for the neutralization mechanism. Differences in simulations from analytic theory are discussed.

I. Introduction

Ion beam neutralization during operation of electric propulsion devices requires both current and charge density matching of the ion beam using an emitted electron beam. This current coupling is easily accomplished in reality, yet the exact process has not been adequately described. Currently an "effective collision frequency" that binds electrons to the ion beam describes the neutralization process[1]. While this can allow for reasonable accuracy in models, it does not explain if we can engineer for this effect or if there are conditions where it does not apply. As electric propulsion becomes more prevalent and new regimes of electric propulsion are explored in space missions, this matter garners significant importance. Proper modeling of current coupling and neutralization will enable development of low-current neutralizers and optimization of neutralizers for micropropulsion devices and clusters of engines. Explanation of the beam coupling mechanism also has bearing on space instrument calibration, electrodynamic tethers, and ionospheric research.

A dense ion beam requires space charge neutralization to avoid a potential barrier that can divert or reflect the beam. The vehicle on which the thruster operates needs current neutrality to avoid unwanted charging. In the context of collisionless plasma theory, achieving both current and charge neutrality with the same source of electrons appears to be nearly impossible owing mostly to the large difference in mass between electrons and the ions. For example, define the ion flux, $F_i = N_i v_i$, and the net electron flux, $F_e = \frac{1}{4} N_e v_{eth}$, where N is density, v is velocity, i and e are ion and electron subscripts and eth designates the electron thermal velocity for an idealized electron source. Equal density and flux requires $v_{eth} = 4v_i$. A 1 keV Xenon beam has v_i=38,000 m/s so a matching electron velocity requires a source temperature of about 0.05 eV. This is a challenging, but not impossible number. However, neutralization is achieved by electrons from thermionic and hollow cathode sources, which do not necessarily provide electrons at such low energies. Of course a higher temperature, lower density electron source will lead to a positive potential well that does trap electrons, but then the theory must explain by what process the trapped electrons shed energy so as to actually fill the well. Since real systems quite easily achieve 'beam coupling,' this suggests that a strong mechanism exists for binding the electrons to the ion beam. Another observation is that when ion beams and neutralizers are operated in conducting vacuum tanks, the currents are closely coupled even

---

* Electronics Engineer, PhD Candidate WPI, Student Member AIAA.
† Tech Advisor, Senior Member AIAA.
‡ Professor, Senior Member AIAA.

though the grounded tank eliminates the charge accumulation that could provide feedback for current balance.[2] One or more plasma mechanisms must be responsible for this collective phenomenon -- charge and current neutrality – which we hereafter call current coupling.

We examine two possibilities for beam neutralization: collisions resulting from Coulomb interactions and revisit the two-stream instability. Ion beams involved in electric propulsion have traditionally been considered collisionless plasma.[3] While standard methods for determining collisionality indicate that the beam should be treated as such, the suggestion of an "effective collision frequency" and the cold ion beam providing a dense "core" of field particles moving at an effectively constant velocity make a detailed analysis necessary. The two-stream instability has been one of the most studied problems in plasma physics. The Buneman Instability[4], also known as the strong beam-plasma instability, is named after a pioneer in the field of plasma simulation that was a leading contributor to early works on ion beam neutralization. Yet the instability has not been declared the solution to the beam neutralization problem. It has been suggested that the instability provides turbulent mixing to fill the electron velocity space, but this creates an electron population traveling at speeds well in excess of the beam velocity. Can either one or some combination of both effects adequately explain current coupling?

II. Coulomb Collisions

For collisions to effectively neutralize an ion beam, they must quickly adjust the electron distribution function to match mean velocities. Since we are interested in distribution functions changing over time, we must use a collision term in the Boltzmann equation. Starting from the Fokker-Plank equation, using the method of Rosenbluth[5], and assuming no external forces or spatial gradients,

$$\left(\frac{\delta f}{\delta t}\right)_{coll} = -\nabla_v\left(\langle \Delta \vec{\mathbf{v}} \rangle f\right) + \sum \frac{1}{2}\frac{\partial^2}{\partial v_r \partial v_s}\left(\langle \Delta v_r \Delta v_s \rangle f\right) \tag{1}$$

where

$$\langle \Delta \vec{\mathbf{v}} \rangle = \sum_s \Gamma_s \nabla_v H_s \tag{2}$$

and

$$\langle \Delta v_r \Delta v_s \rangle = \sum_s \Gamma_s \nabla_v^2 G_s \,. \tag{3}$$

The sum is to be performed on all field species s and the gradient is taken over velocity space. The coefficient Γ is defined as

$$\Gamma_s = \frac{e^4 Z^2 Z_s^2 \ln \Lambda_s}{4\pi\varepsilon_0^2 m^2}, \tag{4}$$

where Z is the charge number and $\ln \Lambda$ is the Coulomb Logarithm. H and G are the Rosenbluth potentials, defined

$$H_s(\vec{\mathbf{v}}) = \frac{m_s}{m_{rs}} \int f_s(\vec{\mathbf{v}}_s)\left|\vec{\mathbf{v}} - \vec{\mathbf{v}}_s\right|^{-1} d\vec{\mathbf{v}}_s = \frac{m_s}{m_{rs}} \int \frac{f_s(\vec{\mathbf{v}}_s)}{u} d\vec{\mathbf{v}}_s \tag{5}$$

and

$$G_s(\vec{\mathbf{v}}) = \int f_s(\vec{\mathbf{v}}_s)\left|\vec{\mathbf{v}} - \vec{\mathbf{v}}_s\right| d\vec{\mathbf{v}}_s = \int f_s(\vec{\mathbf{v}}_s)\, u\, d\vec{\mathbf{v}}_s \,. \tag{6}$$

In the above, f_s is the distribution function of the field species s, velocities $\mathbf{v}_s$ are the velocity coordinates for the field species, m_{rs} is the reduced mass with the field species, and u is the relative velocity between the field species and the test particle. The Rosenbluth potentials behave as velocity-space potentials, similar to electrostatic potentials. It can also be shown that G is the relative number flux distribution between the test particle and the field particles. Rosenbluth potentials give the corrected Coulomb field experienced by the test particle moving through a thermal distribution of field particles. (5) and (6) can be solved for spherical distribution functions (see Appendix) to give

$$H_s = \frac{m_e n \operatorname{erf}\left(\sqrt{x_s}\right)}{m_r v_{ts} \sqrt{x_s}} \tag{7}$$

and

Table 1: Default parameter values.

n	$m_i = m_{Xe}$	T_e	T_i	v_d
1e15	2.18017e-25 kg	1 eV	0.1 eV	38337.2 m/s

$$G_s = \frac{nv_{ts}\left(\sqrt{x_s}\exp(-x_s) + 0.5\sqrt{\pi}\,(2x_s+1)\operatorname{erf}\left(\sqrt{x_s}\right)\right)}{\sqrt{\pi x_s}}. \tag{8}$$

The variable x_s is defined $x_s = v^2/v_{ts}^2$. It is interesting to note that (8) is similar in form to d^2D_+/dx^2 where D_+ is Dawson's Integral, which is related to the Voigt spectral profile: a spectral line broadening due to collisional and thermal motion of the gas being studied.

The relative rate collisions act on the distribution can be described through a collision time, or its inverse, the collision rate. The average momentum collision time for a non-thermal background is well known to be[6]

$$\tau = \frac{v^3}{n_f\Gamma_s} = \frac{1}{\nu}. \tag{9}$$

This can be extended to thermal species by applying the potential function H to the field particle velocity to get

$$\tau_s(\vec{\mathbf{v}}) = \frac{m\vec{\mathbf{v}}}{\Gamma_s\nabla_v H_s}. \tag{10}$$

For multiple species, a total slowing-down time is the sum $1/\tau_{Total} = \sum_s 1/\tau_s = 1/\tau_a + 1/\tau_b + \cdots$, as per Trubnikov[7].

Since the expressions (7) and (8) are only for spherical distributions, we choose a coordinate system where all axes are equivalent for a drifting electron distribution and non-drifting ion distribution to effectively reduce the problem to 1-D. This leads us to use a drift velocity of $v_d' = \sqrt{v_d^2/3}$. Therefore, we have a normalized electron distribution function

$$f_e' = \sqrt{\frac{1}{\pi v_{te}^2}}\exp\left(-\frac{(v+v_d')^2}{v_{te}^2}\right). \tag{11}$$

Using the above equations, the full form of the Fokker-Plank equation can be written. This will enable us to see the change in both the electron distribution function as well as the acceleration of the particles by taking the first moment of the Fokker-Plank equation:

$$\left(\frac{\partial\langle\vec{\mathbf{v}}\rangle}{\partial t}\right)_{coll} = \int\vec{\mathbf{v}}\bullet\left[-\nabla_v\left(\langle\Delta\vec{\mathbf{v}}\rangle f\right) + \sum\frac{1}{2}\frac{\partial^2}{\partial v_r\partial v_s}\left(\langle\Delta v_r\Delta v_s\rangle f\right)\right]d\mathbf{v}. \tag{12}$$

While the integration of (12) is extremely difficult owing to a pole at $v = 0$ and the complex form after derivatives are taken, it can be numerically integrated over a half-space, from near $v = 0$ (avoiding the pole) to ∞ and again on the negative side. We can also look at the shape of the unintegrated curve to see the change any particular particle may be undergoing due to collisions. It is these curves that we are most interested in.

There are only five variables in the expressions for $\left(\partial f/\partial t\right)$ and $\left(\partial\vec{\mathbf{v}}/\partial t\right)$: number density n, ion mass m_i, electron temperature T_e, ion temperature T_i, and electron drift velocity v_d. Using the values in Table 1, equation (1) demonstrates a rapid depletion of electrons near the ion velocities, as shown in blue in Figure 1. Similarly,

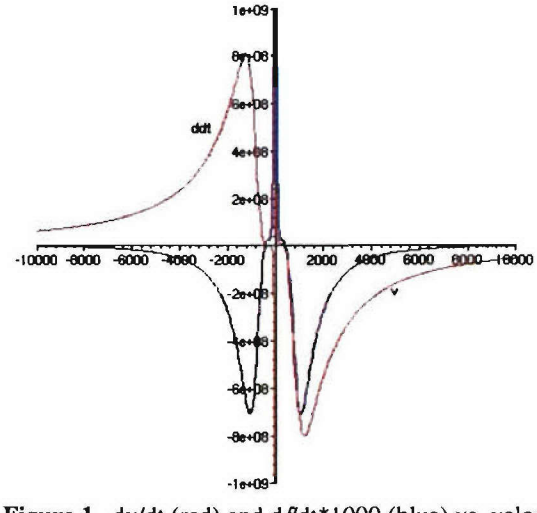

Figure 1. dv/dt (red) and d*f*/dt*1000 (blue) vs. velocity

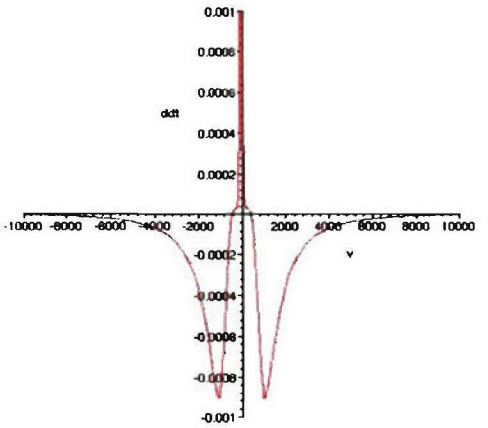

Figure 2. Normalized change in electron distribution function $(df_e/dt)/f$

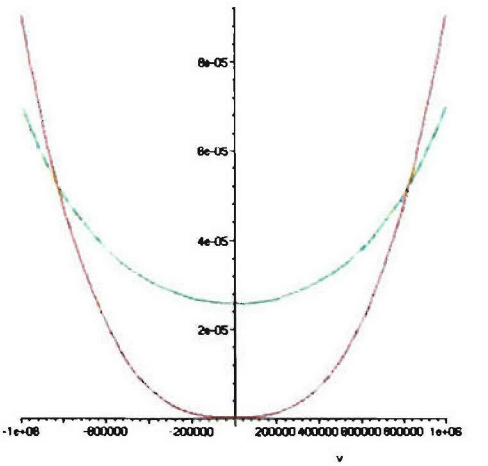

Figure 3: Relaxation Times vs. velocity: red (ion) green (electron).

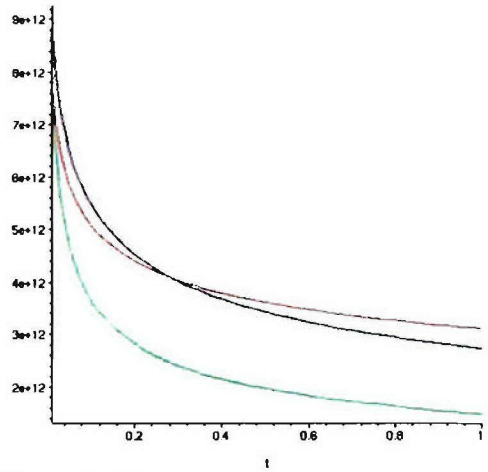

Figure 4: Change in momentum vs. electron temperature (eV) for Ti of 0.1 (red), 1 (blue) and 10 (green) eV.

equation (12) shows acceleration of the electrons in that region towards the beam velocity, shown in red in Figure 1. The vertical axis is in units of m/s^2 for acceleration and particles/second $(nf(v)/s)$ for df/dt. As collisions alone cannot produce a net change in velocity, the two lobes of acceleration are equal and opposite.

When compared to the electron distribution function, the depletion is rather small as shown in Figure 2. However, it does suggest that the beam draws in and does not release electrons that are moving at similar velocities. The rate at which it does this is the question. We next examine the collision time for this event as a function of relative velocity.

Figure 3 shows the collision time as a function of velocity for both electron-electron and electron-ion collisions using equation (10). As can be expected, the electron-electron collisions play a dominant collisional role above approximately the electron thermal velocity, and the ions are the dominant collisional term below that. As the velocity narrows close to the beam velocity, the electron-ion collision time diminishes to as little as 0.1 ns.

Of the parameters listed in Table 1, electron temperature is the one that most dramatically affects the effectiveness of the collisions. This is obvious, as colder distributions will have more electrons with lower relative velocities to ions. The effect can be seen in Figure 4.

Ion temperature does play a role in defining collision times for particles with relative velocities within a few multiples of the ion thermal velocity, but this is small compared to the much larger region of velocity space occupied by the electrons. It is interesting to note, however, that the ions have a maximum momentum transfer to electrons at a given temperature, as seen in Figure 0. This can be understood by realizing that collisions are maximized by reducing the effective collision speed between particles to as low a speed as possible for as many particles as possible. Thus, warmer ions allow the beam to "see" more electrons as slow, thus trapping electrons much more weakly as individuals, but trapping more of them out of the entire distribution. As ion temperature continues increasing, the number of electrons that can be collectively viewed as "slow" also decreases, thus leading to a rapid falloff in the momentum transfer. It will likely be difficult for this effect to be seen experimentally, as the fraction of electrons affected by this is small compared to the overall distribution.

Of the other parameters listed, ion mass plays a small role, with heavier ions containing more momentum to transfer with a given energy. This is also visible in Figure 0. Increasing density also directly increases the probability of collision, as would be expected. As beam velocity for electric propulsion is small compared to electron thermal velocities, it plays a negligible role.

III. The Buneman Instability

The two-stream instability is one of the more commonly studied plasma phenomenon. It is easily modeled via particle-in-cell simulations that have excellent agreement with a

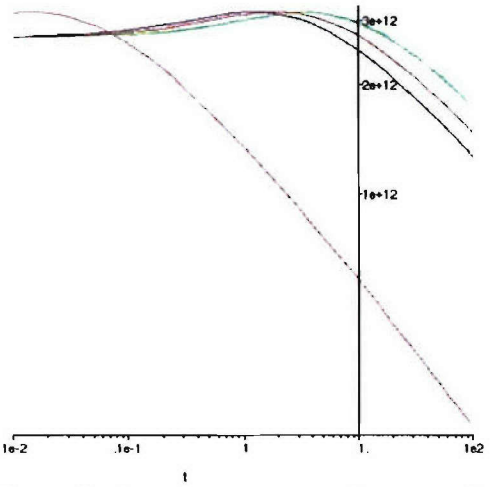

Figure 5: Average momentum change vs. Ion temperature for Radon (green), Xenon (red), Krypton (blue) and protons (magenta).

straightforward analytic solution. The broad instability can be easily broken down into two main subcategories: two-stream, where the interacting elements are simply counterstreaming beams within a neutralizing background; and beam-plasma, where one species is part of the neutralizing background and the other is a perturbation superimposed upon it. It is obvious this can be simply a matter of reference frame adjustment in many cases, but the distinction is significant when one species has a significantly different plasma frequency.

Again, we can break down the beam-plasma instability into two regions: one where the perturbing species plays a minor role in maintaining the quasineutrality of the background, the "weak-beam" model as labeled by Birdsall,[8] and one where the beam is providing a significant portion, if not all, of the charge neutralization for the background – the "strong beam" model. The most extreme version of this, electrons moving through mobile ions, is the Buneman instability.[4] It is this model that we are interested in working with.

We begin with the dispersion relation for an ion and electron plasma, with electrons moving at some speed $\vec{\mathbf{V}}_d$ relative to the ions.

$$1 - \frac{\omega_{pe}^2}{\left(\Omega_k - \vec{\mathbf{k}}\bullet\vec{\mathbf{V}}_d\right)^2} - \frac{\omega_{pi}^2}{\Omega_k^2} = 0 \tag{13}$$

The frequency Ω_k is considered complex but the wavenumber $\vec{\mathbf{k}}$ is real. Introducing the variables $W \equiv \Omega_k/\omega_{pe}$, $K \equiv \vec{\mathbf{k}}\bullet\vec{\mathbf{V}}_d/\omega_{pe}$, and $R \equiv \left(\omega_{pi}/\omega_{pe}\right)^2 = m_e/m_i$, we can write (13) as

$$1 - \frac{1}{(W-K)^2} - \frac{R}{W^2} = 0. \tag{14}$$

Assuming real K and complex W, solutions can be found for variable K. Figure 6 shows three of four roots of (14), with the other root not interacting. The vertical portion of roots one and three is the electron contribution and the horizontal real portion of the roots is the ion contribution. The complex roots show the strongest growth, as expected, at K=1, with this mode quickly dominating. W can be solved at K=1 to give

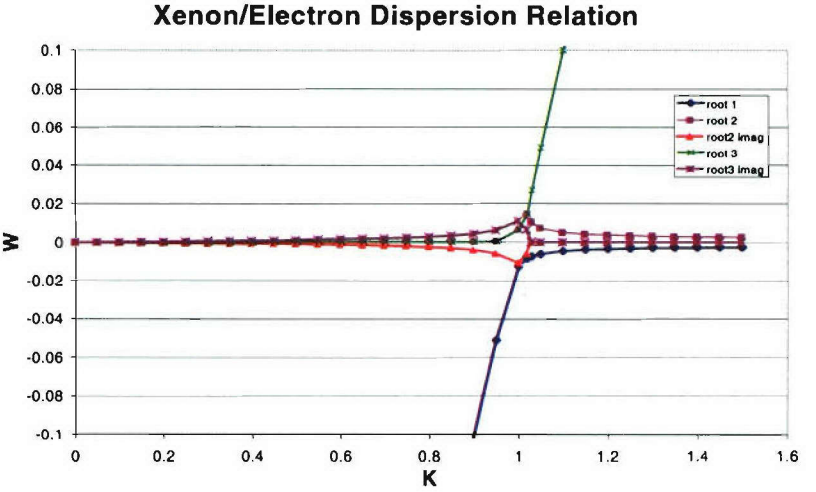

Figure 6: Dispersion Relation for Electron/Xenon Buneman Instability. One root not shown. $W=\omega_{pi}/\omega_{pe}$, $K=kV_d/\omega_{pe}$

$$\Omega_{k=k_{max}} = \omega_k + i\gamma_k$$

$$\omega_{k=k_{max}} = \frac{1}{2}\left(\frac{m_e}{2m_i}\right)^{\frac{1}{3}}\left[1+\frac{1}{2}\left(\frac{m_e}{2m_i}\right)^{\frac{1}{3}}\right]\omega_{pe} \qquad (15)$$

$$\gamma_{k=k_{max}} = \frac{\sqrt{3}}{2}\left(\frac{m_e}{2m_i}\right)^{\frac{1}{3}}\left[1+\frac{1}{2}\left(\frac{m_e}{2m_i}\right)^{\frac{1}{3}}\right]\omega_{pe}$$

Since γ_k is small everywhere except in a narrow range about K=1, any change in the electron velocity will likely produce a significant change in both growth rate and the frequency of the instability. Ishihara, Hirose, and Langdon have produced a series of papers[9,10] that illustrate the growth of this instability and provide an analytical framework to describe its growth and saturation.

In reference 9, a prediction for an effective collision frequency based on the electric field energy density of $\nu_{eff} \simeq 0.53\left(m_e/m_i\right)^{-0.61}\omega_{pe}$ is given. This is obviously far smaller than $\nu_{eff} \cong \omega_{pe}$, which was found by Parks et al.[1] to be approximately the necessary rate to achieve current coupling. As Parks was looking for coupling to match experiment while Ishihara was examining anomalous resistivity, the definitions of effective collision frequency may have been different enough to explain the discrepancy.

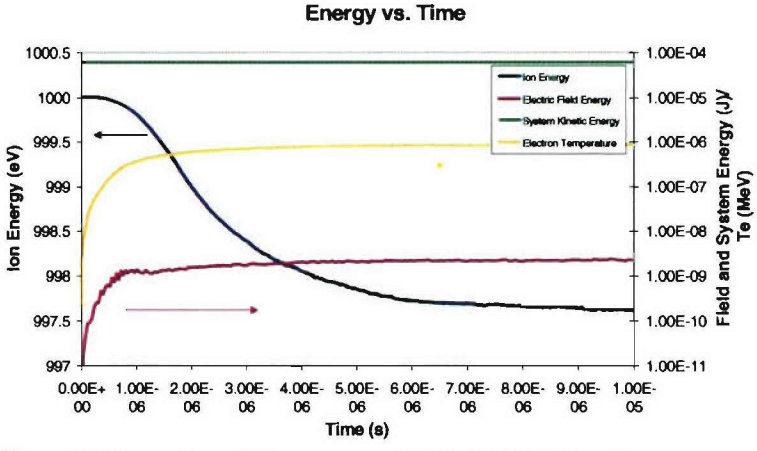

Figure 7: Comparison of ion energy, electric field, total system energy, and electron temperature. Note T_e units on right scale. Reproduced from Figure 13 of Reference 2

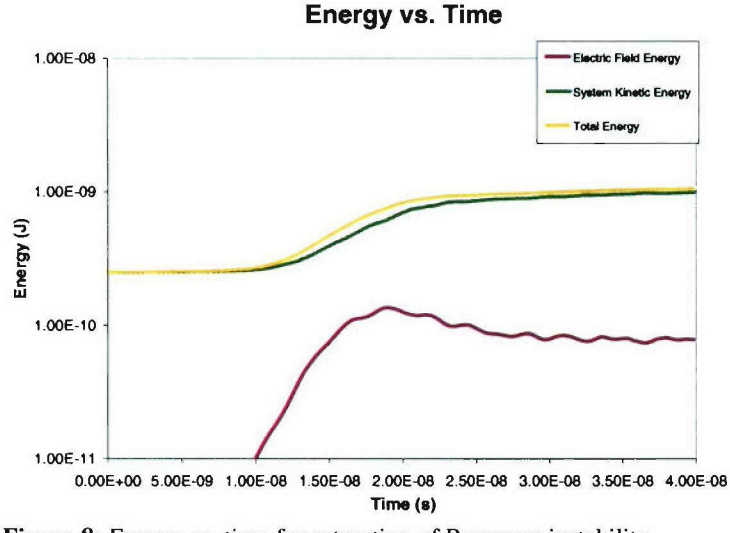

Figure 8: Energy vs. time for saturation of Buneman instability.

Ishihara notes the electric field energy density was shown to grow until saturation at approximately 12% of the initial system energy. This is much higher than the weak beam model in Birdsall[8] and is likely due to the larger role the interactions play in maintaining quasineutrality. The first two higher harmonics were included in both the analytical solution and their simulation with striking agreement. In a previous paper by the authors[2], using the 2-D code XOOPIC[11], it was noted the electric field grew to 0.01% of the system energy, well below the predictions of saturation level given by any two-stream instability theory. The figure illustrating this is reproduced in Figure 7. The discrepancy comes from the fact that the ion kinetic energy was considered the baseline for the system

kinetic energy when in fact it is necessary to only include the electron kinetic energy relative to the ion velocity. If that change of reference frame is established, the resulting system energy changes by a factor of 240,000 and the total system energy in the electric field at saturation is an amazing nine times the initial (relative) kinetic energy.

A plot for a simulation run performed with the reversed viewpoint is shown in Figure 8. Here the energy storage in the electric field grows to 31% of the initial kinetic energy. While more in line with the results suggested above, it is still significantly higher. This discrepancy may be due to the different ion species and the nonperiodic conditions of the simulation.

As in the collision discussion, we are interested not just in the end effects, but in the rate at which the instability grows to saturation. The time to saturation given by Ishihara is approximately 10 growth rate times, or $10\tau_{2s}$, given

$$\tau_{2s} = 1/\gamma \tag{16}$$

with γ from (15). Using the parameters listed in Table 1, (16) gives a time constant of 5.1e-8 s. This is obviously far too long to explain the growth and saturation observed in Figure 8. Assuming the instability growth still follows the same basic rule of $\sim 10\tau_{2s}$ to saturation, an increase in γ of at least an order of magnitude is called for. However, this would provide a growth rate time on the order of ω_{pe}, which matches much more closely the results of Parks.

Reference 10 develops an analytical framework that takes the Buneman instability beyond the saturation point and follows it for several ion time periods. In this time, they observe slow oscillations in the field energy at about ω_{pi}. While the first oscillation is visible in Figure 7 just past the initial saturation point, subsequent oscillations are nonexistent, either damped by thermal particles, or swamped by a growing positive potential well providing electron heating. In Figure 8 the plot does not extend far enough to see these oscillations, but similarly only one cycle was observed. Additionally, the two-dimensional simulation may provide additional degrees of freedom or allow more oscillation modes to coexist, producing "in-the-mean" stability. Finally, ions and electrons were being injected and deleted from the domain throughout the simulation as it was not periodic like those of Ishihara and Hirose. By not maintaining the particles with a "memory" of the instability, the effects may have been dramatically diminished.

The extreme energy storage in the electric field and rapid growth of the instability suggests that there are several differences between the beam simulated for Figure 8 and that simulated by Ishihara et al. The species simulated was different, and as demonstrated in the Coulomb collision discussion, larger mass ions are more effective in giving away momentum. There may also be additional effects involved as the original simulation of Figure 7 showed that more than just the electron kinetic energy was transferred into field energy. Ion heating is a strong possibility for this. Additionally, the beam simulated above was inherently unstable as the potential well was growing, which, if left unchecked, eventually would form a virtual anode to reflect the beam. These virtual anodes were noted previously by the authors.[12]

Net discrepancies between the simulations of this paper and those by Ishihara and Hirose could be due to different simulation parameters, numerical heating, or it could be the numerical "ion pump" effect of bounded simulations as demonstrated by Brieda and Wang[13]. While the "ion pump" instability has been observed in some simulations, the total effect is believed to be small in comparison with the ballistic electrons that remain within the simulation but have energies to move them outside of the beam itself for a period of time. Regardless, if the Buneman instability accurately describes neutralization, the particle mass and periodicity of the simulation should not dramatically impact results.

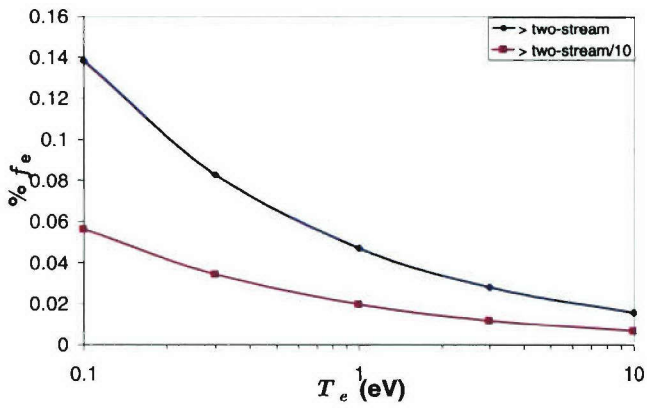

Figure 9: Percent of electron distribution function where $\tau_{cc} > \tau_{2s}$ (blue) and $\tau_{cc} > \tau_{2s}/10$ (magenta)

IV. Comparison and Discussion

In relation to the other dominant mixing agent in the beam, Coulomb collisions still show a stronger effect over a smaller, but still significant, range. Using the time constant from the Buneman instability as given by (16) and τ_{cc} as the ion collision time given from (10), we compare the relative rates of the two.

As noted above, τ_{2s} is approximately 5e-8 s. The relaxation time for coulomb collisions is

variable with velocity. To determine where Coulomb collisions can still be significant, we integrate the electron distribution function between the two points where $\tau_{cc}=\tau_{2s}$. Using the parameters given in Table 1, this still encompasses 4.7% of the electrons. Even $10\tau_{cc}=\tau_{2s}$ covers 2% of the electrons. Varying the electron temperature to cold, but not entirely unphysical levels can produce up to a 13% spread where the collision time is smaller than the growth rate given by (16). This can be seen in Figure 9. Therefore, collisional effects can contribute to a rapid ~1-10% neutralization of the beam, depending on electron temperature. It should be noted that, as mentioned above, the ion temperature has little effect on the collision time over such a large swath of the electron distribution unless at temperatures of several tens of electron volts.

While 10% of the electrons are insufficient to drive neutralization on their own, it still illustrates that collisions can play a non-negligible role in accurately modeling beam neutralization behavior. It also suggests that by providing a very cold electron source one can accelerate the neutralization process.

V. Conclusion

Coulomb collisions can and do play a role in ion beam neutralization. The degree of participation varies dramatically, however, with the thermal energies of the electrons and ions. This is due to the increasing relative velocity over a larger portion of the electron distribution between the electrons and ions. It has been calculated that the portion of neutralization by Coulomb collision could be in excess of 10% depending on beam parameters. Regardless, the small portion of electrons affected and the long timescales needed to collisionally couple electrons with the ion beam suggest strongly that another mechanism is the driving force behind neutralization. This is proposed to be the strong beam-plasma or Buneman instability.

The analytical development of the Buneman instability still shows significant variation from simulated current coupling. Simulations produced a larger electric field energy density and a much quicker growth rate than the analytic theory given by Ishihara et al. Additionally, the ion oscillations were not observed as strongly as expected. These damped quickly, within one cycle. Electron thermalization from a potential well developing in the beam and particle injection and deletion on boundaries are offered as potential reasons.

Appendix: Derivation of Rosenbluth Potential Expressions

To derive the Rosenbluth Potential functions G and H, following Callen[14], we first begin with a spherical distribution function

$$f_s(\mathbf{v}_s)=\frac{n}{(\pi v_{ts})^{3/2}}\exp\left(-v_s^2/v_{ts}^2\right) \tag{A.1}$$

where $v_{ts}=\sqrt{3kT_s/m_s}$ is the thermal velocity. Repeating equations (5) and (6), we have

$$H_s(\mathbf{v})=\frac{m_s}{m_{rs}}\int f_s(\mathbf{v}_s)\left|\mathbf{v}-\mathbf{v}_s\right|^{-1}d\mathbf{v}_s=\frac{m_s}{m_{rs}}\int\frac{f_s(\mathbf{v}_s)}{u}d\mathbf{v}_s \tag{A.2}$$

and

$$G_s(\mathbf{v})=\int f_s(\mathbf{v}_s)\left|\mathbf{v}-\mathbf{v}_s\right|d\mathbf{v}_s=\int f_s(\mathbf{v}_s)u d\mathbf{v}_s\,. \tag{A.3}$$

For both of these, we perform a substitution of $\vec{\mathbf{u}}=\vec{\mathbf{v}}_s-\vec{\mathbf{v}}$. The reason for this shall become clear later, but as $\mathbf{u}$ has the physical meaning of the relative velocity of the two particles, the direction is irrelevant in the collision frame and the only quantity of interest is the magnitude. Using

$$\begin{aligned}v_s^2&=\mathbf{v}_s\bullet\mathbf{v}_s=\mathbf{v}_s\bullet(\mathbf{v}+\mathbf{u})=\mathbf{v}_s\bullet\mathbf{v}+\mathbf{v}_s\bullet\mathbf{u}=(\mathbf{v}+\mathbf{u})\bullet\mathbf{v}+(\mathbf{v}+\mathbf{u})\bullet\mathbf{u}\\&=v^2+u^2+2uv\cos\theta\end{aligned} \tag{A.4}$$

we can write (A.2) and (A.3) as

$$H=\frac{m}{m_{rs}}\frac{n}{\left(\pi v_{ts}^2\right)^{3/2}}\int\frac{\exp\left[-\left(u^2+v^2+2uv\cos\theta\right)/v_{ts}^2\right]}{u}d^3u\,, \tag{A.5}$$

$$G = \frac{n}{\left(\pi v_{ts}^2\right)^{3/2}} \int \exp\left[-\left(u^2 + v^2 + 2uv\cos\theta\right)/v_{ts}^2\right] u d^3u \,. \tag{A.6}$$

It is now necessary to move into spherical coordinates, and using the relation $d(\cos\theta) = \sin\theta d\theta$, we can write

$$H = \frac{m}{m_{rs}} \frac{n}{\left(\pi v_{ts}^2\right)^{3/2}} \int_0^{\infty} \int_{-1}^{1} \int_0^{2\pi} \exp\left[-\left(u^2 + v^2 + 2uv\cos\theta\right)/v_{ts}^2\right] u d\phi d(\cos\theta) du \tag{A.7}$$

$$G = \frac{n}{\left(\pi v_{ts}^2\right)^{3/2}} \int_0^{\infty} \int_{-1}^{1} \int_0^{2\pi} \exp\left[-\left(u^2 + v^2 + 2uv\cos\theta\right)/v_{ts}^2\right] u^3 d\phi d(\cos\theta) du \,. \tag{A.8}$$

While taking the integral over ϕ is trivial, to perform the integration over θ we use the relation

$$\int_{-1}^{1} u \exp\left[-\left(u^2 + v^2 + 2uv\cos\theta\right)/v_{ts}^2\right] d(\cos\theta) = \frac{v_{ts}^2}{2v}\left[\exp\left(-\frac{(v-u)^2}{v_{ts}^2}\right) - \exp\left(-\frac{(v+u)^2}{v_{ts}^2}\right)\right] \tag{A.9}$$

This allows us to write

$$H = \frac{m}{m_{rs}} \frac{n}{\left(\pi v_{ts}^2\right)^{3/2}} \int_0^{\infty} \frac{\pi v_{ts}^2}{v}\left(\exp\left[-\frac{(v-u)^2}{v_{ts}^2}\right] - \exp\left[-\frac{(v+u)^2}{v_{ts}^2}\right]\right) du \tag{A.10}$$

$$G = \frac{n}{\left(\pi v_{ts}^2\right)^{3/2}} \int_0^{\infty} \frac{\pi u^2 v_{ts}^2}{v}\left(\exp\left[-\frac{(v-u)^2}{v_{ts}^2}\right] - \exp\left[-\frac{(v+u)^2}{v_{ts}^2}\right]\right) du \tag{A.11}$$

which can then be integrated to get

$$H = \frac{m}{m_{rs}} \frac{n}{v} \operatorname{erf}\left(\frac{v}{v_{ts}}\right) \tag{A.12}$$

$$G = \frac{n}{v} \frac{v_{ts}^2}{\sqrt{\pi}}\left[\frac{v}{v_{ts}} \exp\left(-\frac{v^2}{v_{ts}^2}\right) + \frac{\sqrt{\pi}}{2}\left(\frac{2v^2}{v_{ts}^2} + 1\right) \operatorname{erf}\left(\frac{v}{v_{ts}}\right)\right]. \tag{A.13}$$

We simplify using $x = v^2/v_{ts}^2$ which matches the results of (7) and (8) with

$$H = \frac{m}{m_{rs}} \frac{n}{v_{ts}\sqrt{x}} \operatorname{erf}\left(\sqrt{x}\right) \tag{A.14}$$

$$G = \frac{n v_{ts}}{\sqrt{x\pi}}\left[\sqrt{x} \exp(-x) + \frac{\sqrt{\pi}}{2}(2x+1) \operatorname{erf}\left(\sqrt{x}\right)\right]. \tag{A.15}$$

It should be noted that these are only first order terms. For non-spherical distribution functions, higher orders can be obtained using spherical harmonics as described by Shkarovsky et al[15].

References

[1] Parks, D.E., Mandell, M.J., Katz, I. "Fluid Model of Neutralized Ion Beams." AIAA 81-0141, 19th Aerospace Sciences Meeting, St. Louis, Missouri, January 12-15, 1981.

[2] Wheelock, A., Cooke, D.L., and Gatsonis, N.A. "Computational Analysis of Current Coupling of Ion Beam-Neutralizer Interactions." AIAA 2005-3692, 41st Joint Propulsion Conference, Tucson, AZ July 10-13, 2005.

[3] Watson, W.K.R. "Justification of the use of the Collisionless Boltzmann Equation for Ion Beam Neutralization Studies." *Progress in Astronautics and Rocketry, Vol. 5: Electrostatic Propulsion*. Langmuir, D., Stuhlinger, E. and Sellen, J.M. Jr (ed), Academic Press, New York, 1961, p.231-235.

[4] Buneman, O. "Dissipation of Currents in Ionized Media." *Phys. Rev.* Vol. 115, No. 3, Aug. 1959, p. 503-517.

[5] Rosenbluth, M., MacDonald, W, and Judd, D. "Fokker-Plank Equation for an Inverse-Square Force." *Physical. Review*, Vol. 107, No. 1, July 1957, p. 1-6.

[6] Miyamoto, K. *Plasma Physics for Nuclear Fusion*. MIT Press, Cambridge, Massachusetts, 1989.

[7] Trubnikov, B. A. "Particle Interactions in a Fully Ionized Plasma." *Reviews of Plasma Physics, Vol. 1*. Leontovich, M.A. (ed), p.105-204, Consultants Bureau, New York, 1965.

[8] Birdsall, C.K., A. B. Langdon, "Plasma Physics via Computer Simulations", *Plasma Physics Series*, 1991.

[9] Ishihara, O., Hirose, A., and Langdon, A.B. "Nonlinear Evolution of Buneman Instability." *Physics of Fluids*, Vol. **24**, No. 3, March 1981 p.452-464.

[10] Hirose, A., Ishihara, O., and Langdon, A.B. "Nonlinear Evolution of Buneman Instability. II. Ion Dynamics." *Physics of Fluids*, Vol. 25, No. 4, April 1982, p.610-616.

[11] Verboncoeur, J.P., Langdon, A.B. and Gladd, N.T. "An Object-Oriented Electromagnetic PIC Code," *Comp. Physics Comm.*, 87, pp. 199-211, May 1995.

[12] Wheelock, A., Gatsonis, N., and Cooke, D. "Ion Beam Neutralization Processes for Electric Micropropulsion Applications" AIAA-2003-5148, 39th Joint Propulsion Conference and Exhibit, Huntsville, AL July 20-23 2003.

[13] Brieda, L. and Wang, J. "Modeling Ion Thruster Beam Neutralization." AIAA 2005-4045, 41st Joint Propulsion Conference, Tucson, AZ July 10-13, 2005.

[14] Callen, J.D. *Fundamentals of Plasma Physics*. In Draft, available at http://homepages.cae.wisc.edu/~callen/, viewed June 2006.

[15] Shkarofsky, I.P. et al. *The Particle Kinetics of Plasmas*. Addison-Wesley Publishing Company, Reading, Massachusetts, 1966.